Trapping of a Coastal Density Front by the Bottom Boundary Layer*

DAVID C. CHAPMAN AND STEVEN J. LENTZ

Woods Hole Oceanographic Institution, Woods Hole, Massachusetts

(Manuscript received 4 November 1992, in final form 2 August 1993)

ABSTRACT

The dynamics of a surface-to-bottom density front on a uniformly sloping continental shelf and the role of density advection in the bottom boundary layer are examined using a three-dimensional, primitive equation numerical model. The front is formed by prescribing a localized freshwater inflow through the coastal boundary. The resulting freshwater plume turns anticyclonically and moves along the coast, generating offshore transport in the bottom boundary layer, which advects freshwater offshore and creates a sharp surface-to-bottom density front with a surface-intensified alongshelf jet over the front. The offshore buoyancy flux in the bottom boundary layer moves the front offshore until it reaches a depth where the vertical shear within the front leads to a reversal in the cross-shelf velocity at the shoreward edge of the front. Consequently, the offshore buoyancy flux in the bottom boundary layer vanishes shoreward of the front. Within the front, a steady balance is established in the bottom boundary layer between vertical mixing and *onshore* advection of density. At this point, the front is "trapped" to an isobath; that is, the front remains parallel to the isobath and does not move farther offshore. The location of the trapped front is consistent with simple thermal wind dynamics. The basic frontal-trapping mechanism dominates the dynamics for a wide range of inflow velocities and densities (including very weak density anomalies), indicating that the advection of density in the bottom boundary layer may play a major role in the circulation on many continental shelves, even when the bottom boundary layer is thin compared to the total water depth.

1. Introduction

Freshwater enters the ocean along many of the world's coastlines from a variety of sources—for example, individual rivers, large estuaries that collect freshwater from several rivers, and meltwater from snow and ice at high latitudes—and typically forms a plume that flows along the coast in the direction of Kelvin wave propagation. Regardless of the freshwater source, the induced shelf circulation tends to occur as one of two dynamically different flows. Often the freshwater forms a shallow, surface-trapped plume that spreads over the ambient shelf water (Fig. 1a), exhibiting strong vertical stratification (e.g., Garvine 1974; Boicourt 1973). These surface-trapped plumes may be strongly affected by ambient shelf flows, winds, and tides, but they are not appreciably influenced by the bottom topography.

In contrast, some freshwater inflows[1] tend to form a plume that spans the water column from surface to bottom (Fig. 1b), creating strong *horizontal* stratification with a surface-to-bottom density front separating the freshwater from the shelf water (e.g., Blanton 1981; Schumacher and Reed 1980; Münchow and Garvine 1993a,b). These surface-to-bottom plumes may be strongly influenced by the bottom topography because much of the plume is in direct contact with the bottom. In particular, the alongshelf flow depicted in Fig. 1b should generate offshore flow of freshwater in the frictional bottom boundary layer, which could push the entire front farther offshore and thereby alter both the density and velocity fields. This potentially important dynamical interaction between the bottom topography and the shelf circulation is the focus of this study.

Dynamical studies of three-dimensional freshwater inflows have concentrated on surface-trapped plumes using a variety of models (e.g., Garvine 1987; O'Donnell 1990; Weaver and Hsieh 1987; Chao 1988), whereas the dynamics of surface-to-bottom freshwater plumes have been largely ignored. Two notable exceptions are the studies of Csanady (1984) and Wright (1989). Csanady (1984) considered a coastal freshwater discharge in a vertically well-mixed ocean over a uniformly sloping bottom. A freshwater plume forms in which the alongshelf advection of freshwater balances horizontal mixing with the ambient shelf water. Wright (1989) studied the movement of a two-layer, surface-to-bottom density front (separating fresher coastal water from denser offshore water) across a constant-depth shelf. In this case, the front continues to

[1] We adopt the ocean view of the freshwater flux, so an *inflow* refers to freshwater *entering* the ocean.

* Woods Hole Oceanographic Institution. Contribution Number 8195.

Corresponding author address: David C. Chapman, Woods Hole Oceanographic Institution, Woods Hole, MA 02543.

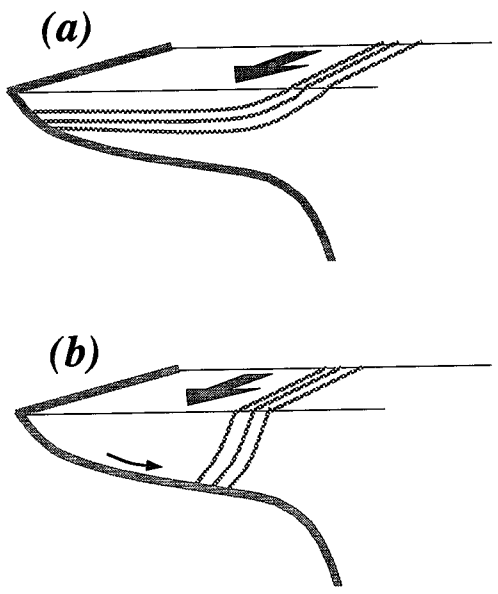

FIG. 1. Sketches depicting (a) a shallow surface-trapped freshwater plume and (b) a surface-to-bottom freshwater plume. The large arrows indicate the direction of the surface currents. The small arrow represents offshore transport in the bottom boundary layer. Case (b) is the subject of study here.

move offshore until the shelfbreak is encountered, whereupon the bottom boundary-layer transport is greatly reduced and the offshore movement of fresher water is nearly halted. Wright (1989) proposed this as a mechanism for the formation of a shelfbreak front.

In both models, the offshore transport in the bottom boundary layer is instrumental in spreading the fresher water over the shelf. However, neither Csanady (1984) nor Wright (1989) allowed a feedback between density advection in the bottom boundary layer and the velocity field. Instead, they each imposed a fixed background flow, which generated the offshore transport in the bottom boundary layer, and then assumed that changes in the flow field associated with the dynamics and motions of the density field remained small compared with the background flow. In essence, they linearized the effect of the bottom boundary layer by allowing it to transport fresher water offshore, while not allowing the transport of density to alter the imposed background flow. Similar linearized treatments, in which the bottom boundary-layer buoyancy transport is not allowed to alter the background density field, are typical of models of shelf dynamics (e.g., Clarke and Brink 1985; Chapman and Brink 1987).

The validity of this linearization assumption is not obvious to us. Can the bottom boundary layer advect stratified fluid in any direction without altering the background stratification and flow? [See, for example, the recent review by Garrett et al. (1993).] If not, what are the dynamical consequences of the feedback between density advection in the bottom boundary layer and the velocity fields? More specifically, how does a surface-to-bottom front behave on a continental shelf if the feedback between density advection in the bottom boundary layer and the velocity field is explicitly allowed? Does the mechanism proposed by Wright (1989) for the formation of a shelfbreak front apply over a sloping bottom in the presence of density advection?

To address these questions concerning the dynamics of a surface-to-bottom density front and the importance of density advection in the bottom boundary layer, we have studied the conceptually simple case of a prescribed localized coastal freshwater source flowing onto a uniformly sloping continental shelf. The freshwater source extends from the surface to the bottom to ensure the interaction, at least initially, with the bottom topography. This imposed source is not intended to model an actual freshwater inflow from an estuary because we have not included any dynamics of the estuary (e.g., a return flow into the estuary). Rather, this source is merely a means for establishing a freshwater plume with a surface-to-bottom density front whose behavior can then be studied in detail. Consequently, we do not focus on the region near the source. We model the flow with a three-dimensional, continuously stratified, primitive equation numerical model (section 2) with fairly simple bottom boundary-layer physics, which allows feedback between the advection of density in the bottom boundary layer and the velocity field. Our primary interest is in the shelf circulation (especially cross-shelf) induced by the freshwater source on long time scales, and not the propagation of the nose of the plume. Therefore, we concentrate on the dynamics of the flow within the plume, well behind the nose, and discuss the development of the steady-state circulation. A typical example of the induced shelf circulation is described in section 3, followed by an exploration of the robustness of the results and a fairly simple interpretation in section 4. The results are discussed in section 5 and summarized in section 6.

2. Numerical model

We use a semispectral primitive equation ocean circulation model, described in detail by Haidvogel et al. (1991), to solve the following hydrostatic momentum, density, and continuity equations:

$$\frac{\partial u}{\partial t} - fv = -\frac{\partial \phi}{\partial x} + \kappa_u \frac{\partial^2 u}{\partial z^2} + D_u \tag{1}$$

$$\frac{\partial v}{\partial t} + fu = -\frac{\partial \phi}{\partial y} + \kappa_u \frac{\partial^2 v}{\partial z^2} + D_v \tag{2}$$

$$\frac{\partial \phi}{\partial z} = -\frac{\rho g}{\rho_0} \tag{3}$$

$$\frac{\partial \rho}{\partial t} + \mathbf{v} \cdot \nabla \rho = \kappa_\rho \frac{\partial^2 \rho}{\partial z^2} \tag{4}$$

$$\frac{\partial u}{\partial x} + \frac{\partial v}{\partial y} + \frac{\partial w}{\partial z} = 0. \tag{5}$$

In this system (u, v, w) represent the (x, y, z) components of the velocity vector $\mathbf{v}$, ρ is the difference between the total density and a constant reference density ρ_0, ϕ is the dynamic pressure (actual pressure divided by ρ_0), f is the Coriolis parameter, g is gravitational acceleration, κ_u is the vertical eddy viscosity, κ_ρ is the vertical eddy diffusivity, and t is time. The variables $D_{u,v}$ represent dissipative functions required for numerical stability.

We have neglected the nonlinear advection of momentum in (1) and (2), but have included the advection of density in (4). This was initially merely a convenience that allowed us to isolate the influence of density advection on the bottom boundary layer and its feedback to the velocity field, while (presumably) avoiding the complications of frontal instabilities. The standard model run described in section 3 has since been repeated with the nonlinear momentum terms included in (1) and (2). The basic evolution of the density and velocity fields is virtually unchanged, although there is an indication of slowly growing instabilities along the density front, the study of which we will leave for future consideration.

The system (1)–(5) is approximated using finite differences in the horizontal, a stretched vertical (sigma) coordinate to handle variations in the bottom topography, and a high-order spectral approximation (an expansion in modified Chebyshev polynomials) to represent the vertical flow structure. A leapfrog–trapezoidal time-stepping scheme is used with an occasional trapezoidal step correction. Haidvogel et al. (1991) give further model details.

The model is configured in a uniformly rotating ($f = 10^{-4}$ s^{-1}) straight channel (Fig. 2) with a coastal wall of depth h_0 at $y = 0$ and an offshore (solid) wall at $y = 200$ km. The channel length is 600 km. The channel is wide enough so that the offshore boundary does not influence the freshwater plume and long enough to allow the plume to develop fully before reaching the boundary at $x = 600$ km. The bottom deepens linearly away from the coast with slope s;

$$h(x, y) = h_0 + sy. \tag{6}$$

The coastal wall depth is taken as $h_0 = 25$ m, while the bottom slope, unless otherwise specified, is $s = 0.001$. There is no flow through the bottom, and a rigid lid is assumed at the surface (i.e., $w = 0$ at $z = 0$). The numerical grid is uniform in the horizontal with 129 alongchannel and 49 across-channel grid points (i.e., $\Delta x = 4.688$ km and $\Delta y = 4.167$ km). Seven Chebyshev polynomials are used to resolve the vertical structure. The model time step is 288 s (1/300 days).

At the surface, the stress is set to zero,

$$\kappa_u \frac{\partial u}{\partial z} = \kappa_u \frac{\partial v}{\partial z} = 0 \quad \text{at} \quad z = 0, \tag{7}$$

and there is no density flux,

$$\kappa_\rho \frac{\partial \rho}{\partial z} = 0 \quad \text{at} \quad z = 0. \tag{8}$$

At the bottom, the shear stress is specified using a linear bottom friction parameterization,

$$\kappa_u \frac{\partial u}{\partial z} = ru \quad \text{at} \quad z = -h \tag{9}$$

$$\kappa_u \frac{\partial v}{\partial z} = rv \quad \text{at} \quad z = -h, \tag{10}$$

where the bottom friction coefficient is set to $r = 0.0005$ m s^{-1}. There is no density flux through the bottom, which becomes

$$\kappa_\rho \frac{\partial \rho}{\partial z} = 0 \quad \text{at} \quad z = -h \tag{11}$$

because of the neglect of horizontal mixing of density in (4).

For simplicity, the vertical mixing coefficients are fixed at $\kappa_u = \kappa_\rho = 0.001$ m^2 s^{-1}. Some of the present calculations have been repeated using a more sophisticated form of the vertical mixing, namely, a Munk and Anderson (1948) parameterization in which the mixing coefficient depends on the local Richardson number, and the results were nearly identical. Additional vertical mixing is applied in the form of instantaneous vertical convective adjustment whenever the water column becomes statically unstable (i.e., when lighter water appears under heavier water). We would prefer to eliminate explicit horizontal mixing entirely; however, some horizontal mixing of momentum is necessary to obtain numerically stable solutions. Therefore, we (rather arbitrarily) choose to apply biharmonic subgrid-scale mixing with a constant mixing coefficient along sigma-coordinate surfaces (i.e., $D_{u,v} = \nu_u \nabla_\sigma^4 u, v$) and use the smallest mixing coefficient that produces a stable calculation, $\nu_u = 5 \times 10^9$ m^4 s^{-1}. There is no horizontal subgrid-scale mixing of density. The free-slip (no stress) boundary condition is applied at the sidewalls, as are no-flux conditions for density and mass.

Each calculation begins from rest. The fluid in the channel is initially homogeneous with $\rho = 0$. At time $t = 0$, a flux of freshwater is imposed through the coast between $x = 187.5$ km and $x = 215.6$ km (Fig. 2) and is held fixed for 120 days of simulation time, by which time the interior flow has essentially reached a steady state. The inflow is uniform from surface to bottom with velocity v_i and density anomaly ρ_i. The upstream boundary is assumed to be a solid wall like the coast and the offshore wall, although a uniform inflow across the entire channel is applied in one calculation (section 4). At the downstream boundary (right end of the channel in Fig. 2), an Orlanski radiation condition is applied to the velocity fields, with a simple advection

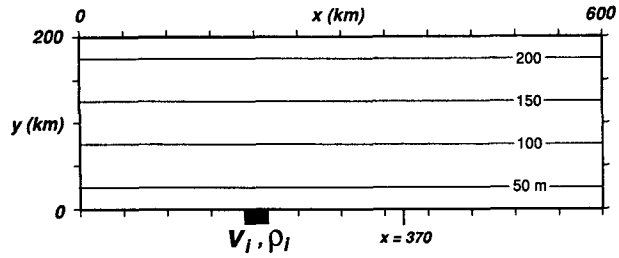

FIG. 2. Model geometry used for the present calculations. An inflow with velocity v_i and density anomaly ρ_i enters the shelf at the solid rectangle along the coast ($y = 0$). The bottom has a uniform slope of $s = 0.001$. Most of the cross-shelf sections presented later are located at $x = 370$ km.

condition applied to the barotropic vorticity field. The application of this open boundary condition is described by Chapman and Haidvogel (1992).

Seven parameters specify each calculation (excluding the horizontal mixing coefficient ν_u). They are the Coriolis parameter f, the bottom friction coefficient r, the bottom slope s, the two vertical mixing coefficients κ_u, κ_ρ, the inflow velocity v_i, and the inflow density anomaly ρ_i. We are particularly interested in the influence of the inflow density anomaly and velocity, so we will generally hold the other five parameters fixed at the values given above.

3. A trapped coastal density front

The behavior of the surface-to-bottom freshwater inflow for the calculation outlined in section 2 is described here using an inflow velocity of $v_i = 0.2$ m s^{-1} and an inflow density anomaly of $\rho_i = -1.0$ kg m^{-3}. The other parameters are set to their standard values given above. The density anomaly is relatively small and represents brackish estuarine water rather than truly fresh water, a choice which emphasizes that advection of even a weak density anomaly within the bottom boundary layer can dramatically alter the shelf circulation. In fact, the flow described below is typical of a wide range of parameter choices (see section 4).

As expected, the freshwater plume primarily turns anticyclonically upon entering the shelf region and, within 2 days, hugs the coast (Fig. 3, upper panel). The nose of the plume, measured by the $\rho = 0.1\rho_i = -0.1$ kg m^{-3} contour, moves fairly steadily along the coast, reaching the end of the channel after about 20 days. The average propagation speed is about 0.23 m s^{-1}, slightly faster than the inflow velocity v_i. Note that some of the freshwater moves along the coast in the opposite direction as well (toward $x = 0$), although at a much slower rate ($\sim$0.02 m s^{-1}). This feature is examined in more detail in section 4. After 30 days, the nose of the freshwater plume has exited the model domain (Fig. 3, lower panel). The plume continues to spread offshore, but the spreading slows with time and, by 120 days, has essentially stopped moving offshore! A steady state has been reached in which the offshore edge of the plume is nearly parallel to the isobaths.

To understand the dynamics of the spreading plume, we examine the evolution of the density and velocity fields at $x = 370$ km. Cross-shelf sections of these variables at times $t = 20$, 30, 60, and 120 days are presented in Fig. 4. The sequence of events is as follows. A thin bottom Ekman layer, with vertical scale $\delta = (2\kappa_u/f)^{1/2} = 4.47$ m, is established soon after the inflow begins to move along the shelf. This generates an offshore transport near the bottom, while a compensating onshore transport develops above the bottom boundary layer, as is apparent in the cross-shelf velocity at $t = 20$ days (upper panels in Fig. 4). The tendency of this cross-shelf circulation is to move fresher (lighter) water under the (heavier) shelf water. This statically unstable situation is quickly rectified by convective adjustment, leading to the homogenization of the water nearest the coast and the establishment of a sharp density front. The density front has a tendency to adjust geostrophically, thereby generating a surface-intensified alongshelf jet with substantial vertical shear that reduces the alongshelf velocity to a small but positive value at the base of the front. The vertical and cross-shelf velocities together define two circulation cells in the cross-front plane, one on each side of the front. The flow is upward on the shoreward side of the front with a downwelling flow near the coast, and downward on the seaward side of the front.

As the inflow continues, the advection of density in the bottom boundary layer (i.e., offshore buoyancy flux)

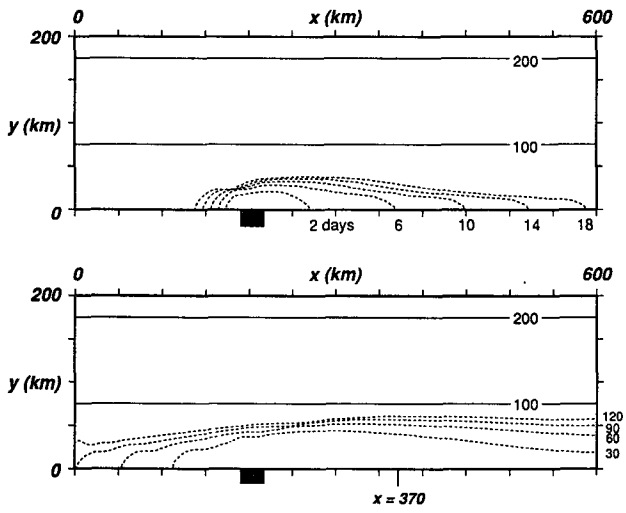

FIG. 3. Plan view of the seaward edge of the freshwater (represented by the $\rho = -0.1$ kg m^{-3} contour at the surface) at times (upper) $t = 2$, 6, 10, 14, and 18 days and (lower) $t = 30$, 60, 90, and 120 days after imposing a freshwater inflow with $v_i = 0.2$ m s^{-1} and $\rho_i = -1$ kg m^{-3}. In both panels, the contour moves offshore with time. The solid rectangle marks the inflow location. The 100- and 200-m isobaths are shown for reference. The entire model domain is shown.

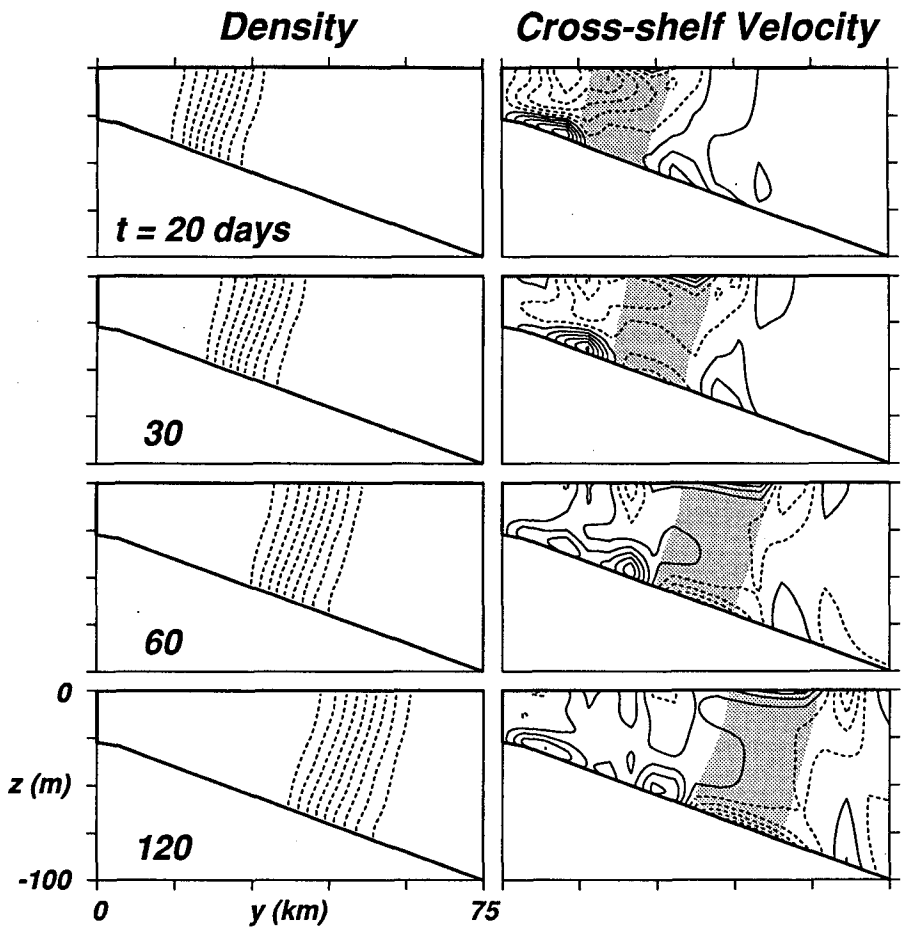

FIG. 4. Cross-shelf sections at $x = 370$ km showing density anomaly (ρ, first column), cross-shelf velocity (v, second column), alongshelf velocity (u, third column), and vertical velocity (w, fourth column) at times $t = 20$ (top row), 30 (second row), 60 (third row), and 120 (bottom row) days after imposing a freshwater inflow with $v_i = 0.2$ m s^{-1} and $\rho_i = -1$ kg m^{-3}. Shading indicates the location of the density front. Contours are -0.9 to -0.1 by 0.1 for density anomaly with

moves the front farther offshore while maintaining nearly identical spatial patterns in the density field and all of the velocity fields ($t = 30$ days; second row of panels in Fig. 4). Each pattern is basically moved intact farther offshore. Most importantly, the width of the density front and the structure of the alongshelf flow (surface velocity and shear) remain nearly constant after 20 days. The primary consequence of the offshore movement, therefore, is that the alongshelf velocity at the bottom has been reduced (and become negative in this case) to the point where the cross-shelf velocity is onshore across most of the base of the density front. This reversal of the cross-shelf transport in the bottom boundary layer reduces the offshore buoyancy flux. The front continues to move offshore but at a slower rate, while the vertical shear in the alongshelf velocity remains roughly constant. Consequently, the region of reversed (negative) cross-shelf flow at the base of the front expands ($t = 60$ days; third row of panels in Fig. 4).

Eventually the front moves into water deep enough that the region of onshore transport in the bottom boundary layer spans the entire base of the front ($t = 120$ days; lowest panels in Fig. 4). At this point, the offshore transport in the bottom boundary layer only occurs shoreward of the front where the density is virtually uniform, so there is no longer an offshore buoyancy flux in the bottom boundary layer and, thus, no mechanism to move the front farther offshore. The net result is that the front must stop at this location; that is, the flow reaches a steady state in which the front is "trapped" along an isobath by the advection of density in the bottom boundary layer!

The trapping mechanism is perhaps best understood by following the evolution of the heat balance (4). The vertical buoyancy flux ($w\partial\rho/\partial z$) is always at least an order of magnitude smaller than the dominant terms in (4) and, therefore, does not contribute to the heat balance. Figure 5 shows cross-shelf sections of the re-

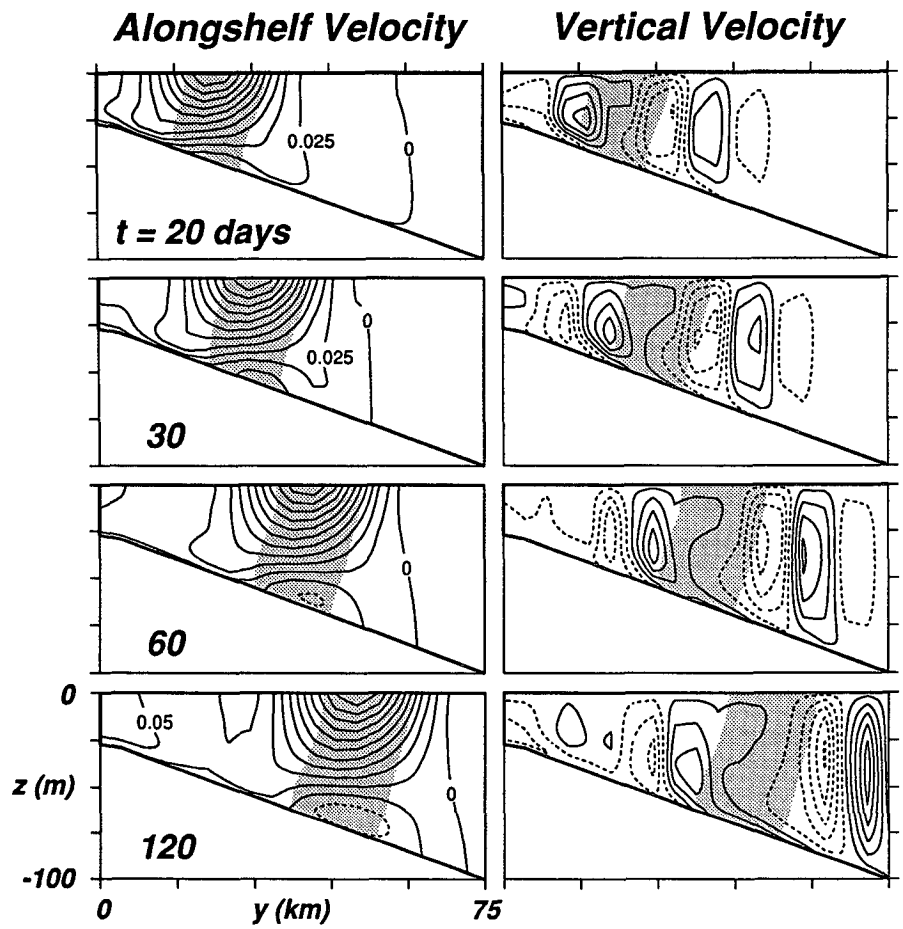

FIG. 4. (*Continued*) the lowest density anomaly at the coast, −0.0225 to 0.0375 by 0.005 for v, −0.025 to 0.275 by 0.025 for u, and -4.5×10^{-5} to 4.5×10^{-5} by 10^{-5} for w. Units are kg m^{-3} for density anomaly and m s^{-1} for the velocities. Solid (dashed) contours are positive (negative) values. Only part of the model domain is shown; $0 < y < 75$ km, -100 m $< z < 0$.

maining terms in (4) at the same times and location as in Fig. 4. Vertical diffusion of density ($\kappa_\rho \partial^2\rho/\partial z^2$, right panels) is a dominant term throughout, basically tending to make the front more vertical, thus being always negative near the bottom and positive near the surface. After 20 days (top row), both the buoyancy flux in the alongshelf ($u\partial\rho/\partial x$) and cross-shelf ($v\partial\rho/\partial y$) directions are substantial, but neither is of the right sign to balance vertical diffusion near the bottom. That is, both are advecting fresher water into the region near the base of the front. The balance is achieved by a decrease in density over the entire frontal region ($\partial\rho/\partial t < 0$), that is, the front moves farther offshore. After 30 days (second row), the region of onshore buoyancy flux near the base of the front ($v\partial\rho/\partial y < 0$) has increased in response to the reversal of the cross-shelf velocity. This begins to balance vertical diffusion, thereby reducing the time rate of change of density. After 60 days (third row), the entire base of the front is within the region of onshore velocity, so the offshore buoyancy flux shoreward of the front has essentially vanished, because the region of offshore velocity is entirely shoreward of the front (see Fig. 4) where the density gradient is nearly zero ($\partial\rho/\partial y \approx 0$). The increased onshore buoyancy flux near the bottom is almost strong enough to balance vertical diffusion, so the density change is very small ($\partial\rho/\partial t \approx 0$).

This evolution continues slowly and by 120 days (bottom row) a steady-state balance is achieved in which the cross-shelf buoyancy flux nearly balances vertical diffusion:

$$v\frac{\partial\rho}{\partial y} = \kappa_\rho \frac{\partial^2\rho}{\partial z^2}. \tag{12}$$

At this point, the front does not move either onshore or offshore, but is "trapped" to this isobath. Cross-shelf buoyancy flux tends to flatten the front, but vertical diffusion tends to make the front more vertical and, thus, prevents the front from being moved onshore

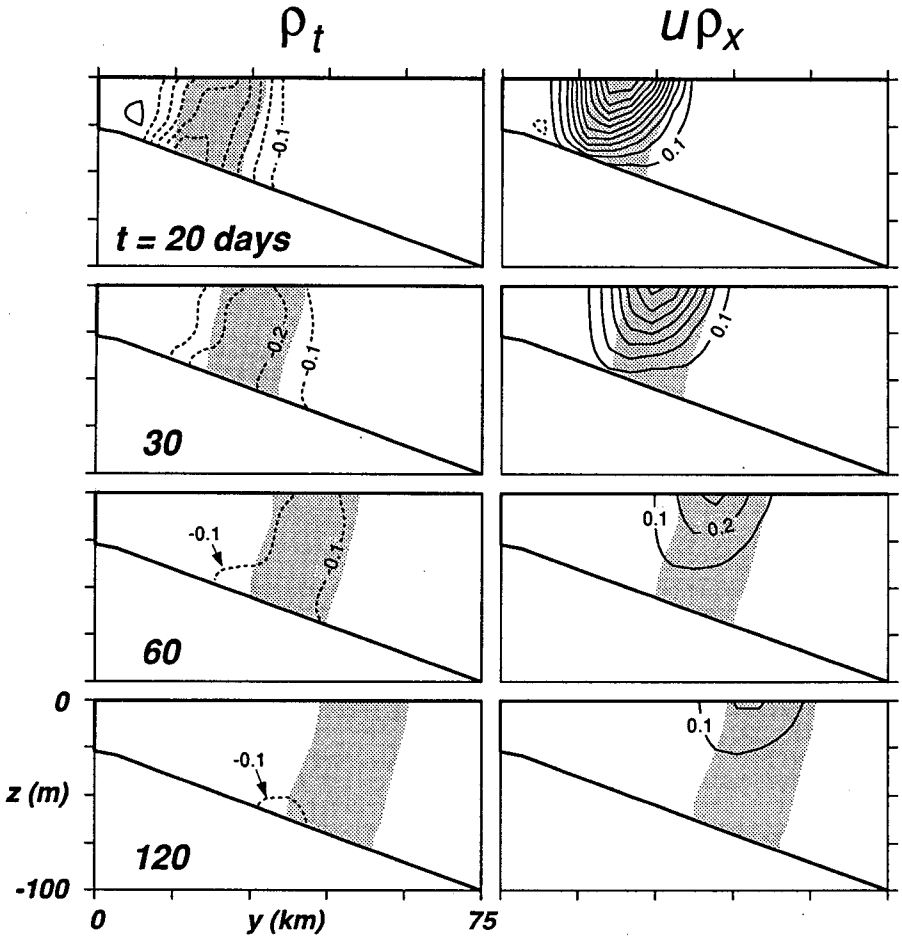

FIG. 5. Cross-shelf sections at $x = 370$ km showing the four dominant terms in the heat balance (4) at times $t = 20$ (top), 30 (second), 60 (third), and 120 (bottom) days after imposing a freshwater inflow with $v_i = 0.2$ m s^{-1} and $\rho_i = -1$ kg m^{-3}. Shading indicates the location of the density front. Contour interval is 0.1×10^{-6} kg m^{-3} s^{-1}. Only part of the model domain is shown; $0 < y < 75$ km, -100 m $< z < 0$.

by the buoyancy flux in the bottom boundary layer. The steady-state balance appears to be a stable equilibrium in the sense that an offshore movement of the front would increase the onshore velocity at the bottom, thus increasing the onshore buoyancy flux and moving the front back toward the trapping location. Likewise, an onshore movement of the front would decrease the onshore velocity at the bottom, thereby decreasing the onshore buoyancy flux and moving the front back toward the trapping location.

The steady-state momentum balances are fairly simple and can be described without illustrations. The alongshelf momentum equation (1) is dominated at the bottom by a balance between the Coriolis term and the vertical diffusion (i.e., the bottom Ekman layer). Away from the boundaries, the alongshelf pressure gradient tends to balance the Coriolis term, although horizontal mixing contributes to the balance near the edges of the front. The cross-shelf momentum balance (2) is nearly geostrophic throughout the water column with an important contribution from the vertical diffusion only near the bottom (i.e., again the bottom Ekman layer).

The trapping of the density front is illustrated in Fig. 6, which shows a plan view at day 120 of the alongshelf velocity maximum at the surface along with two density anomaly contours ($\rho = -0.1$ and -0.9 kg m^{-3}), which represent the seaward and shoreward edges of the density front. The front is narrow and basically remains parallel to the coast with the velocity jet over it. The water shoreward of the front is nearly homogeneous. The important point here is that the freshwater moves only a finite distance offshore. It does not continue to spread offshore either with increasing time or with increasing alongshelf distance. In fact, the only noticeable evolution of this pattern at larger times occurs toward the downstream end of the channel ($x = 600$ km) where the front tends to become more parallel to the coast.

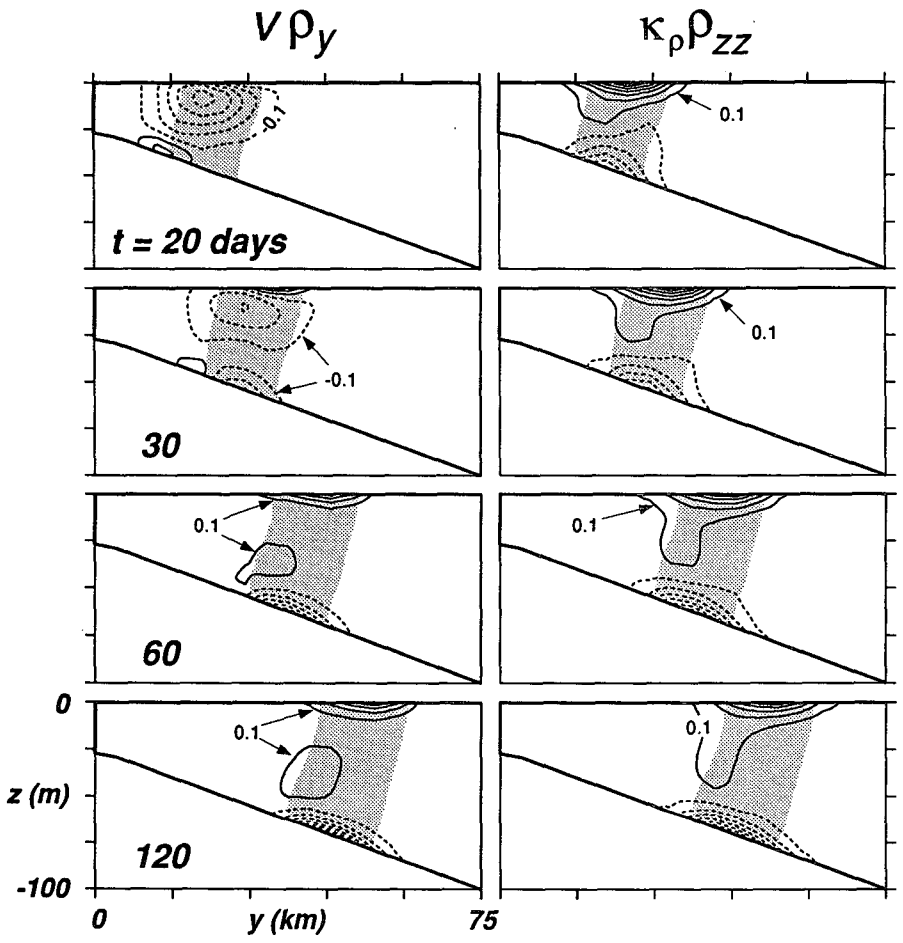

FIG. 5. (*Continued*)

The cross-shelf circulation features shown in Fig. 4—especially the convergence in the bottom boundary layer at the shoreward edge of the density front where the cross-shelf velocity changes sign and the vertical velocity is upward—indicate that the bottom boundary layer separates from the bottom (Gawarkiewicz and Chapman 1992). This can be visualized by following neutrally buoyant particles through the steady-state flow field at day 120. Figure 7 shows the paths of seven particles released 1.36 m above the bottom in the inflow region. The plan view (Fig. 7a) shows that three of the particles move offshore toward the front before turning along the front. Two of the particles move upstream toward $x = 0$, while two others move offshore in complicated curved paths. The vertical motions of the particles are illustrated by a projection of the particle paths onto the cross-shelf plane (Fig. 7b). The three particles that follow the front remain in the bottom boundary layer until they approach the shoreward edge of the front where they are carried vertically upward into the alongshelf jet, indicating a strong connection between the bottom boundary layer and the alongshelf jet; at least some of the transport in the jet is derived from the bottom boundary layer. The two particles that travel upstream move toward the coast and upward suggesting

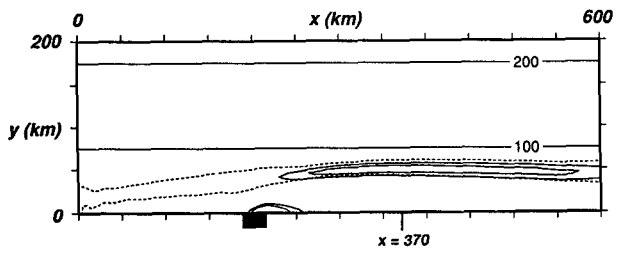

FIG. 6. Plan view of the location of the density front and the alongshelf velocity jet at $t = 120$ days after imposing a freshwater inflow with $v_i = 0.2$ m s^{-1} and $\rho_i = -1$ kg m^{-3}. The dashed curves are the $\rho = -0.1$ kg m^{-3} contour at the surface (farther offshore) and the $\rho = -0.9$ kg m^{-3} contour at the surface (closer to the coast), which represent the edges of the density front. The solid curves are the $u = 0.2$ and 0.25 m s^{-1} contours at the surface, which locate the maxima in u. The solid rectangle marks the inflow location. The 100- and 200-m isobaths are drawn for reference. The entire model domain is shown.

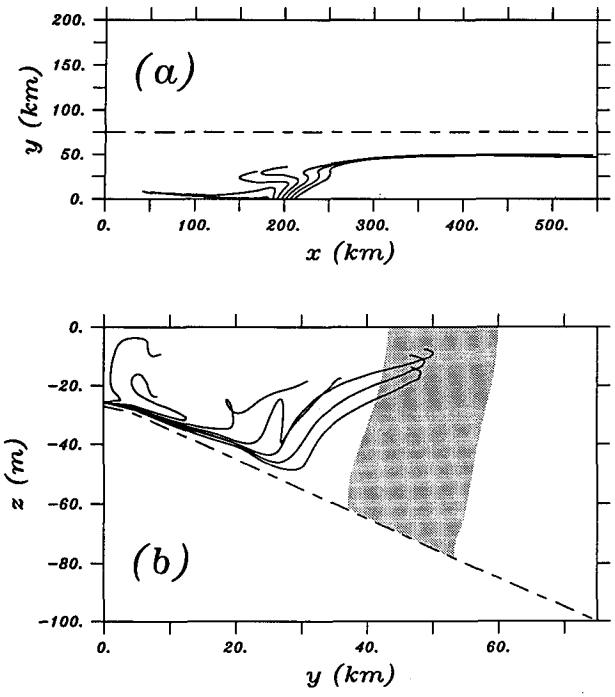

FIG. 7. Paths of seven neutrally buoyant particles projected on (a) the $x - y$ plane and (b) the $y - z$ plane. The flow shown in Fig. 6 and the bottom panels of Fig. 4 was held fixed, and the particles were released into this flow at different alongshelf locations within the freshwater inflow, 1.36 m above the bottom. Three of the particles in (a) tend to follow the high velocity jet shown in Fig. 6. The rapid vertical motion of the three most offshore paths in (b) occurs near the shoreward edge of the density front (shaded region). The dashed line in (a) is the 100-m isobath. Only part of the model domain is shown: $0 < x < 550$ km, $0 < y < 200$ km in (a); $0 < y < 75$ km, -100 m $< z < 0$ in (b).

a very different flow regime, which will be described briefly in section 4. The other two particles again show complicated paths with considerable vertical motion. The important point is that none of these particles escapes onto the seaward side of the front, indicating that the bottom boundary layer does indeed separate from the bottom and that there is little transport across the front. The freshwater inflow is effectively isolated from the deeper shelf water.

4. Generalizations

The results presented in the previous section illustrate the behavior of a surface-to-bottom freshwater plume and the resulting density front on a uniformly sloping shelf for a particular choice of inflow variables and other parameters. In this section, we examine the plume and frontal dynamics for a variety of parameter choices in order to generalize the results and establish the robustness of our interpretation.

Our hypothesis is that the offshore buoyancy flux in the bottom boundary layer moves the density front offshore to the point where the cross-shelf velocity vanishes at the shoreward edge of the base of the front. At this location, the cross-shelf velocity is onshore across the entire base of the front, so the front is no longer being pushed offshore by density advection in the bottom boundary layer. To check the consistency of this argument, we consider the steady form of (1) and neglect lateral mixing (i.e., we set $\partial u/\partial t = 0$ and $D_u = 0$). Integrating vertically through the bottom boundary layer of thickness δ yields

$$-f\int_{-h}^{-h+\delta} v\,dz = -\delta\frac{\partial\phi}{\partial x} + \kappa_u\frac{\partial u}{\partial z}\bigg|_{-h}^{-h+\delta}, \qquad (13)$$

where $\partial\phi/\partial x$ has been assumed constant within the bottom boundary layer. If the stress is confined to the bottom boundary layer, then $\kappa_u\partial u/\partial z \approx 0$ at $z = -h + \delta$. The stress at the bottom is given by (9), so (13) becomes

$$-f\int_{-h}^{-h+\delta} v\,dz = -\delta\frac{\partial\phi}{\partial x} - ru_b, \qquad (14)$$

where u_b is the alongshelf velocity at the bottom. Within the frontal region, the alongshelf velocity is nearly geostrophic (i.e., $fu \approx -\partial\phi/\partial y$) and decreases almost linearly with depth from a surface maximum. Using the hydrostatic balance (3) to obtain the thermal wind relation $[\partial u/\partial z = (g/f\rho_0)\partial\rho/\partial y]$, the velocity at the bottom may be approximated by

$$u_b = u_{\max} - h\frac{g}{f\rho_0}\frac{\partial\rho}{\partial y}. \qquad (15)$$

We expect the front to be trapped at the location of vanishing cross-shelf velocity, that is, $v = 0$. It is interesting to note from (14) that this condition may be met without a reversal in the alongshelf velocity because of the contribution of the alongshelf pressure gradient. This situation occurs in the case of an upstream inflow discussed below. Substituting (15) into (14), setting $v = 0$ and using the bottom topography (6), we can solve for the location of the shoreward edge of the trapped front,

$$y_f = \frac{f\rho_0}{sg}\frac{u_{\max}}{\partial\rho/\partial y}\left(1 + \frac{\delta\partial\phi/\partial x}{ru_{\max}}\right) - \frac{h_0}{s}. \qquad (16)$$

Several features of (16) are worth pointing out. First, the effect of the alongshelf pressure gradient is to decrease y_f because $\partial\phi/\partial x$ is always negative in the frontal region. However, this term is typically small, less than about 4% in all cases presented here, so it can be neglected. This means that the front should be located close to where the alongshelf velocity reverses as well as where the cross-shelf velocity reverses. Second, if the pressure gradient term is small, then an increase in the alongshelf jet velocity ($u_{\max}$), a decrease in the cross-frontal density gradient ($\partial\rho/\partial y$), or a decrease in bottom slope (s) each should increase the offshore location of the front (i.e., the front should be located farther

from the coast). Third, the bottom friction coefficient and the vertical mixing coefficient appear only in the small alongshelf pressure gradient term (κ_u enters through δ). Therefore, the frontal location should be relatively insensitive to the magnitude of these coefficients despite the fact that both processes represented by them are necessary for the steady-state balance to occur. Finally, we hasten to point out that (16) is not a prediction of the frontal location but rather a consistency check because we have not presented any way of predicting $u_{\max}$ or $\partial\rho/\partial y$ based on, for example, the inflow velocity and density anomaly.

We compute y_f from (16) by taking the maximum alongshelf velocity in the jet to be $u_{\max}$ and approximating $\partial\rho/\partial y$ using the distance between the $\rho = 0.2\rho_i$ and $\rho = 0.8\rho_i$ contours at $z = -25$ m depth. For the standard flow described in section 3, the cross-shelf velocity is zero at the bottom at $y_0 = 35.7$ km while the estimate from (16) is $y_f = 33.6$ km. Both of these offshore distances are close to the location of the shoreward edge of the density front (where the $\rho = 0.9\rho_i$ surface intersects the bottom), $y_s = 37.1$ km. So, our simple explanation for the final location of the front appears to hold.

A scaling analysis of the heat balance (12) is also revealing. As above, we consider the steady form of (1) and this time neglect both lateral mixing and the (small) alongshelf pressure gradient, so $v \approx -(\kappa_u/f)\partial^2 u/\partial z^2$. This and thermal wind can be substituted into the left side of (12) to yield

$$-\left(\frac{\kappa_u \rho_0}{g}\right)\frac{\partial^2 u}{\partial z^2}\frac{\partial u}{\partial z} = \kappa_\rho \frac{\partial^2 \rho}{\partial z^2}. \qquad (17)$$

This is the steady balance proposed by Garrett and Loder (1981), except that we have neglected the vertical advection of density. Next we scale u by v_i, ρ by ρ_i, and z by h_0 to obtain

$$-\left(\frac{\kappa_u}{\kappa_\rho}\right)F^2 \frac{\partial^2 u}{\partial z^2}\frac{\partial u}{\partial z} = \frac{\partial^2 \rho}{\partial z^2}, \qquad (18)$$

where u, ρ, and z are now scaled variables and

$$F = \frac{v_i}{(g\rho_i h_0/\rho_0)^{1/2}}$$

is the inflow Froude number. This scaling implies that the behavior of the steady front should be a function of the inflow Froude number; that is, the effect of varying v_i and ρ_i should combine in this form. We now examine the above interpretations for a variety of parameter choices.

a. *Inflow velocity*

According to (16), the offshore location of the density front should increase with increased alongshelf velocity maximum $u_{\max}$. Intuitively, we expect that an increase in v_i should increase $u_{\max}$ and place the front farther offshore, although we do not know the details of the relationship between v_i and $u_{\max}$. This intuition is confirmed in Fig. 8, which shows a plan view of the $\rho = 0.1\rho_i = -0.1$ kg m^{-3} contour at $t = 120$ days for four different inflow velocities, $v_i = 0.1$, 0.2, 0.3, and 0.4 m s^{-1}. All other parameters are identical to those used in section 3. As v_i increases, the front is indeed trapped farther from the coast. Nevertheless, the front is trapped regardless of the inflow velocity, and the flow patterns (not shown) are qualitatively unchanged.

A more quantitative view of the influence of v_i, as well as the robustness of (16), is presented in Table 1 (cases A). The maximum alongshelf velocity, $u_{\max}$, indeed increases with increasing v_i, but not very rapidly. A fourfold increase in v_i only increases $u_{\max}$ by a factor of 1.5. The vertical shear, on the other hand, is only weakly dependent on v_i. The shoreward edge of the front y_s is always nearly coincident with the location of the cross-shelf velocity reversal y_0, indicating that the bottom boundary layer separates from the bottom at the shoreward edge of the front. Both of these distances are estimated fairly accurately by y_f, as computed from (16), although the difference increases with increasing v_i.

b. *Inflow density anomaly*

Based on the dominance of density advection in the bottom boundary layer, we may anticipate that a smaller inflow density anomaly (i.e., smaller $|\rho_i|$) would produce a smaller horizontal density gradient, which according to (16), should place the front farther from the coast. In the limiting case of an inflow with no density anomaly ($\rho_i = 0$), there is no buoyancy flux in the bottom boundary layer, so the plume should exhibit no trapping at all.

Figure 9 shows the seaward extent of the plume at $t = 120$ days in plan view for four different inflow density anomalies, $\rho_i = 0$, -0.1, -0.5, and -1 kg m^{-3}. All other parameters are the same as for the case described in section 3. For the unstratified case, $\rho_i = 0$, a transport streamline is used to delineate the seaward edge of the

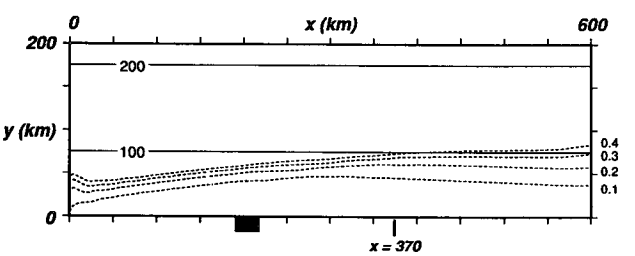

FIG. 8. Plan view of the seaward edge of the freshwater plume (represented by the $\rho = -0.1$ kg m^{-3} contour at the surface) at $t = 120$ days after imposing a freshwater inflow with $\rho_i = -1$ kg m^{-3} and four different inflow velocities, $v_i = 0.1$, 0.2, 0.3, and 0.4 m s^{-1}. The solid rectangle marks the inflow location. The 100- and 200-m isobaths are shown for reference. The entire model domain is shown.

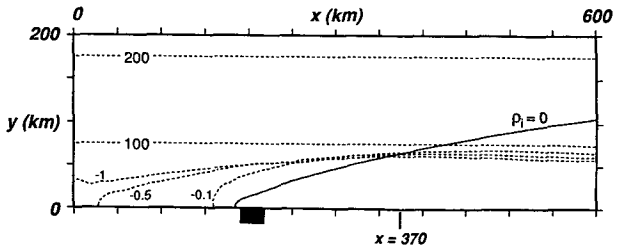

FIG. 9. Plan view of the seaward edge of the freshwater plume at $t = 120$ days after imposing a freshwater inflow with $v_i = 0.2$ m s^{-1} and four different inflow densities, $\rho_i = 0, -0.1, -0.5$, and -1 kg m^{-3}. The seaward extent of the inflow is represented by a transport streamline ($\psi = 5000$ m^3 s^{-1}) for the $\rho_i = 0$ case, and by the $\rho = 0.1\rho_i$ contour at the surface for the others. Downstream of the inflow, the front is closer to the coast for a fresher inflow (i.e., larger $|\rho_i|$). The solid rectangle marks the inflow location. The 100- and 200-m isobaths are shown for reference. The entire model domain is shown.

inflow because there are no density contours. For the other cases, the $\rho = 0.1\rho_i$ contour is drawn. Clearly, when there is no density anomaly ($\rho_i = 0$), no front is formed and the inflow is not trapped, but rather continues to move offshore as it moves downstream. This is basically the arrested topographic wave solution (Csanady 1978) without the long-wave assumption. It is also nearly identical (except for the offshore boundary condition) to one of the cases studied by Woods and Beardsley (1988). The cross-shelf flow patterns at $x = 370$ km for this case (Fig. 10) are considerably different from those for the standard case (bottom panels of Fig. 4). There is no density front, so there is no vertical shear associated with it. The only vertical shear present in u results from bottom friction. There is no reversal in the cross-shelf flow at the bottom, so the offshore transport continues unimpeded, decreasing in deeper water only because the water was initially at rest. The bottom boundary layer does not separate from the bottom; continuity is maintained by the turning of the flow along the shelf.

The most remarkable feature of Fig. 9 is that even a small density anomaly dramatically alters the flow compared with the homogeneous case ($\rho_i = 0$), creating the trapped density front described in section 3, yet the final location of the front is only weakly dependent on ρ_i. This is illustrated for a wider range of density anomalies in Table 1 (cases B). The weak dependence on ρ_i stems from the fact that a change in the inflow density anomaly changes both the vertical shear and the maximum alongshelf velocity, effects that offset in (16). The change in vertical shear is slightly greater, but not so much that it dominates. Thus, the change in the frontal location is small. Table 1 also shows that the shoreward edge of the front again nearly coincides with the cross-shelf velocity reversal ($y_s \approx y_0$), and the frontal location, y_f, estimated from (16) is again in rather good agreement with both. Furthermore, in all of the cases with nonzero density anomaly, the flow patterns are qualitatively identical to those described in section 3.

The frontal locations presented in Table 1 for variations in both inflow density anomaly and velocity are plotted in Fig. 11. As suggested by the scaling in (18), the location of the trapped front, measured either by the zero in cross-shelf velocity or by the shoreward edge of the density front, is clearly a function of the inflow Froude number (all else being equal), although the functional relationship is unclear. The trapping location increases slowly with increasing inflow velocity or decreasing inflow density anomaly. That is, even a very small inflow density anomaly or a very large inflow velocity will severely limit the offshore movement of the front. (Of course, the linearization of the momentum equations is suspect for large inflow velocities.) The asterisks in Fig. 11 are the estimates of the frontal location based on (16), which are quite close for small Froude numbers, but less accurate for $F > 0.6$.

c. *Upstream inflow*

We have neglected the effects of the ambient shelf circulation on the evolution of the freshwater plume. Yet, it is not unusual for a freshwater inflow to encounter a mean alongshelf flow with a magnitude

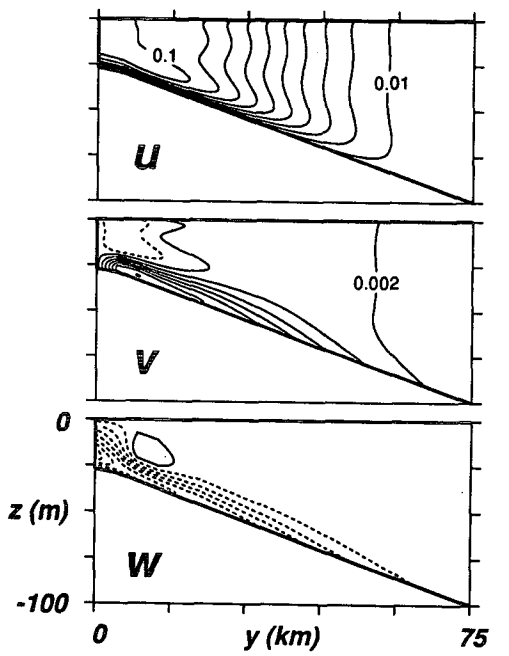

FIG. 10. Cross-shelf sections at $x = 370$ km showing the alongshelf velocity (top), cross-shelf velocity (middle), and vertical velocity (bottom) at $t = 120$ days after imposing a freshwater inflow with $v_i = 0.2$ m s^{-1} and $\rho_i = 0$, i.e., no density variation. Contours are 0.01 to 0.1 by 0.01 for u with the maximum at the coast, -0.002 to 0.026 by 0.004 for v, and -3.75×10^{-5} to 0.75×10^{-5} by 0.5×10^{-5} for w. All units are m s^{-1}. Only part of the model domain is shown; $0 < y < 75$ km, -100 m $< z < 0$.

TABLE 1. Frontal characteristics at $x = 370$ km for various inflow density anomalies ρ_i and velocities v_i: u_{max} is the maximum alongshelf velocity in the frontal jet; u_z is an estimate of the vertical shear based on the horizontal distance between the $\rho = 0.8\rho_i$ and $\rho = 0.2\rho_i$ contours at 25-m depth; y_s is the shoreward edge of the front given by the location where $\rho = 0.9\rho_i$ intersects the bottom; y_0 is the location where the cross-shelf velocity goes to zero at the bottom; y_f is the location of the shoreward edge of the front estimated from (16). Case C includes a uniform upstream inflow of 0.05 m s^{-1}. Case D uses a bottom slope of $s = 0.002$. Case E uses a bottom friction coefficient of $r = 0.001$ m s^{-1}. Case F uses a vertical mixing coefficient of $\kappa_u = \kappa_\rho = 0.002$ m^2 s^{-1}. Units are kg m^{-3} for density anomaly, m s^{-1} for the velocities, 10^{-2} s^{-1} for the vertical shear, and km for the distances.

	ρ_i	v_i	u_{max}	u_z	y_s	y_o	y_f	Remarks
A	−1	0.1	0.216	0.436	22.9	21.4	24.5	
	−1	0.2	0.275	0.469	37.1	35.7	33.6	
	−1	0.3	0.306	0.487	43.3	42.7	37.8	
	−1	0.4	0.323	0.497	47.3	46.9	40.0	
B	−0.1	0.2	0.054	0.075	51.1	52.3	46.7	
	−0.25	0.2	0.101	0.152	47.3	47.8	41.6	
	−0.5	0.2	0.170	0.264	43.1	42.6	39.4	
	−1	0.2	0.275	0.469	37.1	35.7	33.6	
	−1.5	0.2	0.345	0.632	32.4	31.2	29.6	
	−2	0.2	0.418	0.789	28.4	26.3	28.0	
C	−1	0.2	0.338	0.565	28.9	28.9	34.8	inflow of 0.05 m s^{-1}
D	−1	0.2	0.297	0.429	22.2	21.4	22.1	$s = 0.002$
E	−1	0.2	0.274	0.478	38.1	36.7	32.3	$r = 0.001$ m s^{-1}
F	−1	0.2	0.273	0.460	39.7	38.4	34.3	$\kappa_u = \kappa_\rho = 0.002$ m^2 s^{-1}

comparable to the inflow velocity. This is the case, for example, along the Middle Atlantic Bight where a mean alongshelf flow of 0.05–0.1 m s^{-1} toward the southwest occurs over most of the shelf (e.g., Beardsley and Boicourt 1981). Such a flow generates an offshore transport in the bottom boundary layer, which could affect the development of the freshwater plume. In fact, both Csanady (1984) and Wright (1989) assumed that such a mean alongshelf flow provides the offshore transport in the bottom boundary layer, which dominates the cross-shelf circulation and moves the freshwater offshore. They further assumed that the mean alongshelf flow was unaltered by the freshwater inflow, that is, there was no feedback between the density field and the mean alongshelf flow.

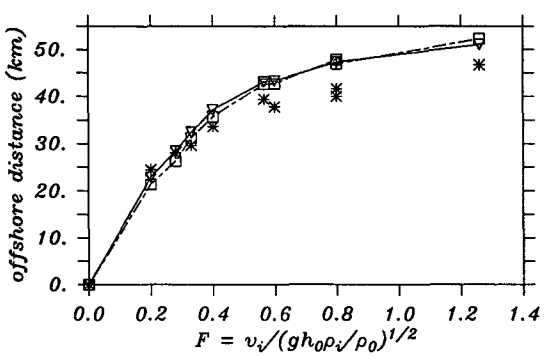

FIG. 11. Offshore location of the trapped density front measured by the intersection of the $\rho = 0.9\rho_i$ contour with the bottom (triangles), the zero of the cross-shelf velocity at the bottom (squares), and estimated from (16) (asterisks) for various inflow Froude numbers. Actual values are listed in Table 1.

If these assumptions are valid, then we would expect the addition of a mean alongshelf flow to move the density front farther offshore. To examine this possibility, we have repeated the calculation described in section 3, but now with a uniform alongshelf velocity of 0.05 m s^{-1} imposed at the upstream boundary ($x = 0$). The resulting steady-state freshwater plume is delineated in Fig. 12 by the $\rho = -0.1$ and -0.9 kg m^{-3} contours and the alongshelf velocity maxima at the surface. Comparing the location of the front with the case described in section 3 (see Fig. 6 and Table 1), we see two important differences. First, the upstream inflow has eliminated the spreading of the freshwater along the coast toward the upstream boundary. Second, and more importantly, rather than moving the front farther offshore, the upstream inflow has slightly *reduced* the offshore location of the front!

This may be understood as follows. Independent of the freshwater inflow, the imposed upstream inflow must have an ageostrophic component of the alongshelf

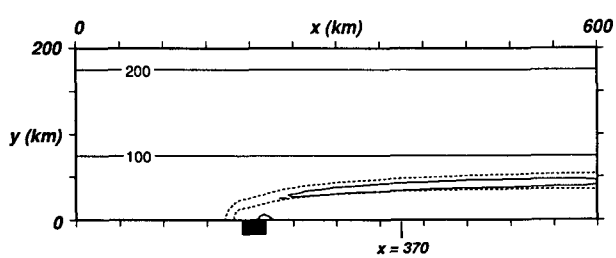

FIG. 12. As in Fig. 6 except that a uniform alongshelf flow of 0.05 m s^{-1} has been imposed across the entire channel at the upstream boundary ($x = 0$). The velocity contour (solid curve) is 0.3 m s^{-1}.

pressure gradient ($\partial\phi/\partial x$) to balance the bottom stress. This pressure gradient extends through the water column (including the bottom boundary layer) contributing an onshore geostrophic velocity that tends to push the density front shoreward and increase the horizontal density gradient (i.e., vertical shear). Figure 13 shows that the density front at $x = 370$ km is closer to the coast, more vertical, and slightly narrower than the standard case in Fig. 4 (see Table 1, case C). The corresponding vertical shear is larger, which means that the cross-shelf velocity at the shoreward edge of the front reverses in shallower water. Once the flow across the entire base of the front is shoreward, then the balance (12) obtains and the front is trapped, despite the presence of offshore flow in the bottom boundary layer seaward of the front. In fact, the alongshelf pressure gradient from the upstream inflow allows the cross-shelf velocity at the bottom to reverse without a reversal in the alongshelf velocity (Fig. 13), consistent with a significant contribution from $\partial\phi/\partial x$ in (16). The estimate of the trapping location based on (16) neglecting the alongshelf pressure gradient term (Table 1, case C) is substantially larger than the actual frontal location, indicating the importance of $\partial\phi/\partial x$. Nevertheless, the circulation is qualitatively identical to the cases without an upstream inflow, once again illustrating the robustness of the underlying dynamics and frontal-trapping mechanism.

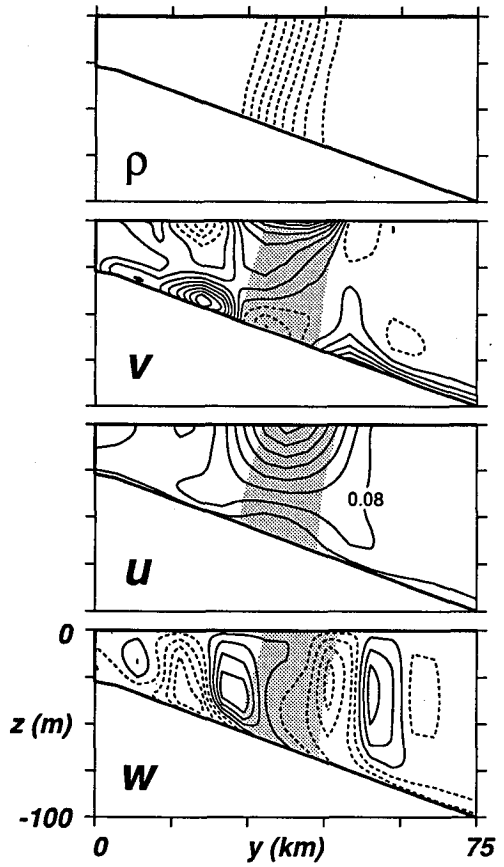

FIG. 13. Cross-shelf sections at $x = 370$ km showing the density anomaly (top), cross-shelf velocity (second), alongshelf velocity (third), and vertical velocity (bottom) for the flow shown in Fig. 12. Shading indicates the location of the density front. Contours are -0.9 to -0.1 by 0.1 for density anomaly with the lowest density anomaly at the coast, -0.0125 to 0.0425 by 0.005 for v, 0.04 to 0.32 by 0.04 for u, and -3.5×10^{-5} to 4.5×10^{-5} by 10^{-5} for w. Units are kg m^{-3} for density anomaly and m s^{-1} for the velocities. Only part of the model domain is shown; $0 < y < 75$ km, -100 m $< z < 0$.

d. *Bottom slope, bottom friction, and vertical mixing*

The effects of changing the bottom slope, the bottom friction coefficient, and the vertical mixing coefficients have also been examined. All else being equal, (16) suggests that a steeper bottom slope will lead to trapping of the density front closer to the coast because, for a fixed vertical shear, the reversal in the cross-shelf velocity will occur closer to the coast. We have demonstrated this by repeating the calculation described in section 3 with twice the bottom slope, $s = 0.002$. Again we find that (16) provides a good estimate of the frontal location (Table 1, case D) and that the circulation is qualitatively unchanged (not shown).

The bottom friction and vertical mixing coefficients enter (16) only in the alongshelf pressure gradient term, which is generally small. So we may expect the steady flow to be insensitive to these parameters. We have confirmed this by repeating the calculation of section 3, once with $r = 0.001$ m s^{-1} and once with $\kappa_u = \kappa_\rho = 0.002$ m^2 s^{-1}, and have found that the flow and frontal trapping are almost unchanged (Table 1, cases E and F).

e. *Upstream propagation*

As mentioned in section 3 and shown in Fig. 3, a curious feature of the shelf response is that some of the freshwater inflow moves upstream along the coast toward the boundary at $x = 0$. The plume moves slowly upstream with an average velocity of only about 0.02 m s^{-1}, one tenth of the inflow velocity v_i. An examination of the momentum balances near the beginning of the calculation reveals that the front "self-advects" along the shelf. The initial geostrophic adjustment produces an upstream velocity ($u < 0$) near the coast on the upstream side of the inflow. This produces a positive buoyancy flux ($u\partial\rho/\partial x > 0$) that is balanced by a density decrease ($\partial\rho/\partial t < 0$). (Vertical density mixing is negligible at this time.) Thus, the front starts to move upstream. The nearly geostrophic frontal jet then carries fluid away from the wall, and this flow is replaced by an upstream flow along the bottom, originating at the inflow. The resulting alongshelf flow continues to provide a positive buoyancy flux, which then continues the upstream propagation. This explanation is supported by Fig. 9, which shows that the

rate of upstream movement is highly dependent on the inflow density anomaly, and hence the density gradient across the front. The upstream propagation is drastically reduced for the weakest density anomaly.

When the plume reaches the solid boundary at $x = 0$, the freshwater is slowly pushed offshore. This is potentially worrisome because it might affect the steady-state flow and the downstream location of the density front. However, we have demonstrated that this is not the case by moving the freshwater inflow location down the channel and repeating the calculation described in section 3. The resulting flow near the upstream boundary is indeed altered, but the flow downstream is virtually identical. Most importantly, the offshore location of the density front and the cross-shelf circulation (not shown here) are unchanged. Furthermore, we do not expect the upstream propagation to be terribly important because it is entirely eliminated by a fairly weak mean alongshelf flow (Fig. 12) typical of many ocean shelves. Thus, it is unlikely that the upstream propagation would be observed except, perhaps, in special circumstances.

5. Discussion

We have shown that the basic dynamics and resulting circulation described in section 3 are quite robust, developing for a wide range of parameter choices. The flow development and steady state are qualitatively unchanged by different inflow velocities and density anomalies, the presence of an ambient shelf circulation and changes in bottom slope, bottom friction coefficient, and vertical mixing coefficient. Additional preliminary results (not presented here) show that vertical density stratification of the ambient shelf water does not qualitatively alter the results either. Therefore, it is useful to consider some of the implications of the results with regard to our understanding of circulation on continental shelves.

First and foremost, the results demonstrate the importance (and perhaps dominance) of density advection in the bottom boundary layer. For more than a decade, much of our intuition and understanding of low-frequency and steady shelf circulation has been built upon linear models that ignore density advection in the bottom boundary layer. One example is the simple, yet elegant, conceptual model of the arrested topographic wave (Csanady 1978) and its numerous extensions. In particular, these depth-averaged barotropic models have revealed the importance of bottom friction (i.e., the bottom boundary layer) in generating cross-shelf transport, despite the fact that the bottom boundary layer is not explicitly resolved. Other linear models have improved our understanding of the wind-driven shelf response (e.g., Clarke and Brink 1985) and the effects of offshore forcing (e.g., Chapman and Brink 1987), but they have treated the bottom boundary layer as an infinitesimal layer that does not modify the ambient density stratification.

Recently, however, Gawarkiewicz and Chapman (1991) have shown that the depth-averaged barotropic models may lead to serious misinterpretations of the actual three-dimensional circulation, precisely because of their failure to resolve the bottom boundary-layer flow explicitly. Gawarkiewicz and Chapman (1992) showed that ambient density stratification, also neglected in the depth-averaged barotropic models, can qualitatively alter the flow obtained for a homogeneous fluid, primarily through the advection of density in the bottom boundary layer. In the present study, we have isolated the bottom boundary-layer effect in a simpler setting than that considered by Gawarkiewicz and Chapman (1992) and shown that density advection in the bottom boundary layer can have a fundamental influence on the shelf circulation. Our results suggest that attempts to include the effects of density advection in the bottom boundary layer by linearization (i.e., assuming that its effects are of secondary importance) are inappropriate. That is, a linear limit may not be attainable because the advection of very small density variations still dominates the flow, producing lowest-order changes in the circulation (see Fig. 9). We conclude that the flow associated with a surface-to-bottom density front over a continental shelf is fundamentally nonlinear, and that it is time to move beyond the purely linear models (e.g., the arrested topographic wave), despite their attractive simplicity, and develop conceptual models that include density advection in the bottom boundary layer. We should no longer ignore the feedback between the density and velocity fields.

The present results show that an important consequence of density advection in the bottom boundary layer is the possibility of trapping buoyancy-driven flows on the continental shelf. Without the feedback between buoyancy advection in the bottom boundary layer and the velocity field, an alongshelf flow is inevitably carried seaward until it eventually leaks off the shelf and mixes with slope water [e.g., the arrested topographic wave or Wright's (1989) model]. However, the dynamics described here provide a mechanism for maintaining buoyancy-driven coastal flows on the shelf over very long distances, for example, along much of the east coast of North America as proposed by Chapman and Beardsley (1989). There is no need to appeal to external forces to oppose the offshore flow in the bottom boundary layer, such as an alongshelf pressure gradient of deep-sea origin (e.g., Chapman et al. 1986). Rather, this mechanism is inherent in the local dynamics of coastal flow.

Another implication concerns the formation of shelfbreak fronts. It has been suggested that a shelfbreak front may form by the continuous inflow of freshwater onto the shelf (e.g., Kao 1981) and/or the movement of a density front across the shelf (e.g., Wright 1989). The present results show that this is unlikely unless the shelfbreak is closer to the coast than the trapping lo-

cation (i.e., a narrow shelf). Otherwise, the density front will be trapped before reaching the shelfbreak.

Finally, we have concentrated on an idealized scenario and have ignored some aspects of the dynamics and the forcing, all of which have been assumed to be of secondary importance. For instance, we have considered the simplest parameterization of vertical mixing, that is, constant mixing coefficients. There are numerous more sophisticated treatments, which might have some effect on the flows presented here. As mentioned above, a parameterization of mixing based on the approach of Munk and Anderson (1948), in which the mixing coefficients depend on the ambient stratification and the vertical shear, had virtually no effect on the results. Other choices, such as a higher-order turbulence closure scheme or the PWP model (Price et al. 1986) remain to be tested.

Numerous other generalizations could also be made. As mentioned earlier, nonlinear advection of momentum may lead to instabilities of the basic flow described above, which could produce significant eddy exchanges across the front. Temporal variations of the freshwater inflow will certainly alter the frontal position. In fact, the steady state may be viewed as the maximum offshore location of the front under sustained maximum inflow. Seasonal or other reductions in the inflow should move the front closer to the coast. Wind forcing may move the density front across the shelf and would presumably drive some frontal exchange. Alongshelf variations in the ambient shelf circulation and bottom topography are also candidates for altering the steady flows presented here. The importance of each of these processes is left for future consideration.

6. Summary

We have examined the dynamics of a surface-to-bottom freshwater plume on a uniformly sloping continental shelf. The freshwater plume primarily turns anticyclonically until it hugs the coast where it then propagates along the shelf. The alongshelf flow produces offshore transport in the bottom boundary layer that homogenizes the water near the coast, thereby maintaining a surface-to-bottom density front. The density front adjusts geostrophically, generating a surface-intensified alongshelf jet over the front and strong vertical shear associated with it. The bottom boundary layer continues to transport buoyancy offshore, which moves the entire front offshore. Eventually the front moves into water deep enough that the vertical shear causes a reversal in the cross-shelf flow across the entire base of the front, thus eliminating the offshore buoyancy flux in the bottom boundary layer. At this point, the density front stops moving offshore and is, in effect, "trapped" along an isobath by the advection of density in the bottom boundary layer. The bottom boundary layer separates from the bottom at the shoreward edge of the front, and effectively closes off the circulation within the freshwater plume. These dynamics dominate the shelf circulation for a range of inflow velocities and density anomalies, even a very small density anomaly of 0.1 kg m^{-3}, suggesting that density advection in the bottom boundary layer is of fundamental importance in shelf flows.

Acknowledgments. Numerous valuable discussions with Glen Gawarkiewicz (WHOI) during the course of this research are much appreciated. We also thank Rich Garvine (U. of Delaware) and Joseph Atkinson (SUNY at Buffalo) for their insightful questions and comments. Financial support was provided by the National Science Foundation under Grants OCE88-16015, OCE91-15713, and DPP91-13940. Computer facilities at the National Center for Atmospheric Research in Boulder, Colorado, were essential for the numerical calculations. The National Center for Atmospheric Research is funded by the National Science Foundation.

REFERENCES

Beardsley, R. C., and W. C. Boicourt, 1981: On estuarine and continental-shelf circulation in the Middle Atlantic Bight. *Evolution of Physical Oceanography,* B. A. Warren and C. Wunsch, Eds., The MIT Press, 198–233.

Blanton, J. O., 1981: Ocean currents along a nearshore frontal zone on the continental shelf of the southeastern United States. *J. Phys. Oceanogr.,* **11,** 1627–1637.

Boicourt, W. C., 1973: The circulation of water on the continental shelf from Chesapeake Bay to Cape Hatteras. Ph.D. thesis, The Johns Hopkins University, Baltimore, MD, 183 pp.

Chapman, D. C., and K. H. Brink, 1987: Shelf and slope circulation induced by fluctuating offshore forcing. *J. Geophys. Res.,* **92,** 11 741–11 760.

——, and R. C. Beardsley, 1989: On the origin of shelf water in the Middle Atlantic Bight. *J. Phys. Oceanogr.,* **19,** 384–391.

——, and D. B. Haidvogel, 1992: Formation of Taylor caps over a tall isolated seamount in a stratified ocean. *Geophys. Astrophys. Fluid Dyn.,* **64,** 31–65.

——, J. A. Barth, R. C. Beardsley, and R. G. Fairbanks, 1986: On the continuity of mean flow between the Scotian Shelf and the Middle Atlantic Bight. *J. Phys. Oceanogr.,* **16,** 758–772.

Chao, S.-Y., 1988: River-forced estuarine plumes. *J. Phys. Oceanogr.,* **18,** 72–88.

Clarke, A. J., and K. H. Brink, 1985: The response of stratified, frictional flow of shelf and slope waters to fluctuating large-scale, low-frequency wind forcing. *J. Phys. Oceanogr.,* **15,** 439–453.

Csanady, G. T., 1978: The arrested topographic wave. *J. Phys. Oceanogr.,* **8,** 47–62.

——, 1984: Circulation induced by river inflow in well mixed water over a sloping continental shelf. *J. Phys. Oceanogr.,* **14,** 1703–1711.

Garrett, C. J. R., and J. W. Loder, 1981: Dynamical aspects of shallow sea fronts. *Phil. Trans. Roy. Soc. London,* **A302,** 563–581.

——, P. MacCready, and P. Rhines, 1993: Boundary mixing and arrested Ekman layers: Rotating stratified flow near a sloping boundary. *Ann. Rev. Fluid Mech.,* **25,** 291–323.

Garvine, R. W., 1974: Physical features of the Connecticut River outflow during high discharge. *J. Geophys. Res.,* **79,** 831–846.

——, 1987: Estuary plumes and fronts in shelf waters: A layer model. *J. Phys. Oceanogr.,* **17,** 1877–1896.

Gawarkiewicz, G., and D. C. Chapman, 1991: Formation and maintenance of shelfbreak fronts in an unstratified flow. *J. Phys. Oceanogr.,* **21,** 1225–1239.

——, and ——, 1992: The role of stratification in the formation and maintenance of shelfbreak fronts. *J. Phys. Oceanogr.*, **22,** 753–772.

Haidvogel, D. B., J. L. Wilkin, and R. Young, 1991: A semi-spectral primitive equation ocean circulation model using vertical sigma and orthogonal curvilinear horizontal coordinates. *J. Comput. Phys.*, **94,** 151–185.

Kao, T. W., 1981: The dynamics of oceanic fronts. Part II: Shelf water structure due to freshwater discharge. *J. Phys. Oceanogr.*, **11,** 1215–1223.

Münchow, A., and R. W. Garvine, 1993a: Dynamical properties of a buoyancy driven coastal current. *J. Geophys. Res.*, **98,** 20 063–20 078.

——, and ——, 1993b: Buoyancy and wind forcing of a coastal current. *J. Mar. Res.*, **51,** 293–322.

Munk, W. H., and E. R. Anderson, 1948: Notes on a theory of the thermocline. *J. Mar. Res.*, **7,** 276–295.

O'Donnell, J., 1990: The formation and fate of a river plume: A numerical model. *J. Phys. Oceanogr.*, **20,** 551–569.

Price, J. F., R. A. Weller, and R. Pinkel, 1986: Diurnal cycling: Observations and models of the upper ocean response to diurnal heating, cooling, and wind mixing. *J. Geophys. Res.*, **91,** 8411–8427.

Schumacher, J. D., and R. K. Reed, 1980: Coastal flow in the northwest Gulf of Alaska: The Kenai current. *J. Geophys. Res.*, **85,** 6680–6688.

Weaver, A. J., and W. W. Hsieh, 1987: The influence of buoyancy flux from estuaries on continental shelf circulation. *J. Phys. Oceanogr.*, **17,** 2127–2140.

Woods, A. W., and R. C. Beardsley, 1988: On the barotropic discharge of a homogeneous fluid onto a continental shelf. *Contin. Shelf Res.*, **8,** 307–327.

Wright, D. G., 1989: On the alongshelf evolution of an idealized density front. *J. Phys. Oceanogr.*, **19,** 532–541.